Chapter 6

INVESTIGATIONS OF NANOCRYSTALLINE CU5NI95 ALLOY PARTICLES BY *IN SITU* TEY XAFS, *IN SITU* XRD AND XPS

6.1. Introduction

Alloys of Cu and Ni have attracted the interest of the surface science and catalysis research communities for more than 50 years [1-5]. They have been commonly regarded as important model systems for the study of promotion effects in bimetallic catalysts. In addition, Cu/Ni alloys have also been shown to exhibit interesting catalytic activity of which only the steam conversion of methane and a variety of hydrogenation and dehydrogenation reactions involving alkanes, olefins and aromatic compounds [6-9] shall be mentioned.

Fundamental surface science studies over the full composition range as well as catalytic studies of small dispersed particles have provided strong evidence that the surfaces of these alloys are generally Cu enriched when compared to the bulk composition. Surface segregation of one bulk constituent in bimetallic alloys is a common phenomenon [10-13] and has, in the case of Cu/Ni alloys, been discussed in terms of the onset of phase separation [6].

Relevant experimental studies of single crystal Cu/Ni alloy surfaces and their interaction with adsorbates have made use of electron spectroscopies, ion scattering techniques, time-of-flight atom probe field ionisation microscopy (TOF FIM) and desorption techniques, while theoretical work has been performed with a variety of calculation schemes [14-37]. With the exception of the TOF-FIM work by Sakurai *et al.* [38-40] all studies have concluded that Cu segregates over the whole range of bulk compositions and orientations of single crystal Cu/Ni alloy surfaces. There is some disagreement with respect to the extent of Cu enrichment in the equilibrium alloy surfaces. Measured values of Cu surface concentrations on alloys containing 5at% of Cu very between 60at% and 96at% [20,22,36]. Different results are expected for different surface orientations.

Surface reactivity studies with dispersed Cu/Ni alloys [6,8,41-59] have provided strong evidence that surface segregation also occurs in small particles. Moreover, the presence of particle-support interactions does not impede the segregation process,

provided that the loading of the catalyst is high. For low loadings on oxidic supports the formation of mixed oxides during calcination has been observed (see ref. [44], and references therein).

The work described in this chapter is concerned with Cu$_5$Ni$_{95}$ alloy particles and the effect of Cu segregation on the Cu and Ni K-edge TEY XAFS of the dispersed material. The surface segregated layer provides an experimental check for the surface sensitivity of the TEY technique as applied to dispersed materials. Complementary structural and surface information on the gas-surface interaction has been obtained using *in situ* XRD and by XPS measurements in a UHV apparatus coupled to a high (p $< 10^{-3}$ atm) pressure vessel.

6.2. Experimental

The dispersed Cu$_5$Ni$_{95}$ alloy sample was prepared from an aqueous solution of Cu(NO$_3$)$_2$ (99.9% pure) and Ni(NO$_3$)$_2$ (99.8% pure) in the desired molar ratio. The particle precursor was precipitated at 60°C from a 1.5 molar nitrate solution by the slow addition of 1 molar NaOH until neutrality was reached. The light green precipitate was filtered through a Büchner funnel and washed four times with ultra-deionised water. It was calcined overnight in ambient air at 110°C and subsequently reduced under a stream of pure hydrogen applying a constant temperature gradient from 25°C to 220°C over a period of two hours. After ramping the temperature, the alloy was allowed to sinter in H$_2$ for a further 2 h at 220°C. The black metal powder was then removed from the furnace and used for *in situ* EXAFS, XPS and XRD investigations without further treatment. The elemental composition of particles was subsequently checked by energy-dispersive X-ray microanalysis (EDX), which yielded a Cu content of 5.7% $\pm$ 0.3%. No other elemental signals were found within the sensitivity range of EDX (0.5%). After preparation, the samples were stored in glass vials at room temperature.

XAFS experiments were carried out in the *in situ* TEY cell described in section 2.6. Synchrotron radiation from beamline 8.1 of the EPSRC Daresbury Laboratory was used, with the storage ring operating at 2 GeV. Ring currents varied between 140 mA and 240 mA. The details of the XAFS and XRD measurement conditions were identical to those described in chapter 5. The powdered alloy was slurried onto the sample plate as a dispersion in deionised water, and dried at room temperature. Gases used in the experiments included He (Distillers MG 99.99%), H$_2$ (BOC, 99.99%) and blended air (99.9% pure, 80% N$_2$ / 20% O$_2$ mixture).

Complementary XPS measurements were performed on a thick pressed pellet (approx. 0.5 mm) of the alloy particles mounted onto a Pt foil sample holder. The VG ADES (angle-dispersive electron spectroscopy) system used for these measurements is coupled to a high-pressure cell which, in principle, allows gas exposures at atmospheric pressure. Leak problems with the Viton seal of the environmental cell limited the maximum working pressure with H_2 to the 10^{-3} mbar region. These H_2 pressures proved too low to reduce the surface of the sample *in situ*, presumably because water formed in the background volume of the environmental chamber competes for reaction at the alloy surface. All reduction treatments were therefore carried out thermally in UHV. The base pressure of the UHV-system was in the high 10^{-10} mbar region thoughout all XPS measurements. The energy scale of the XP
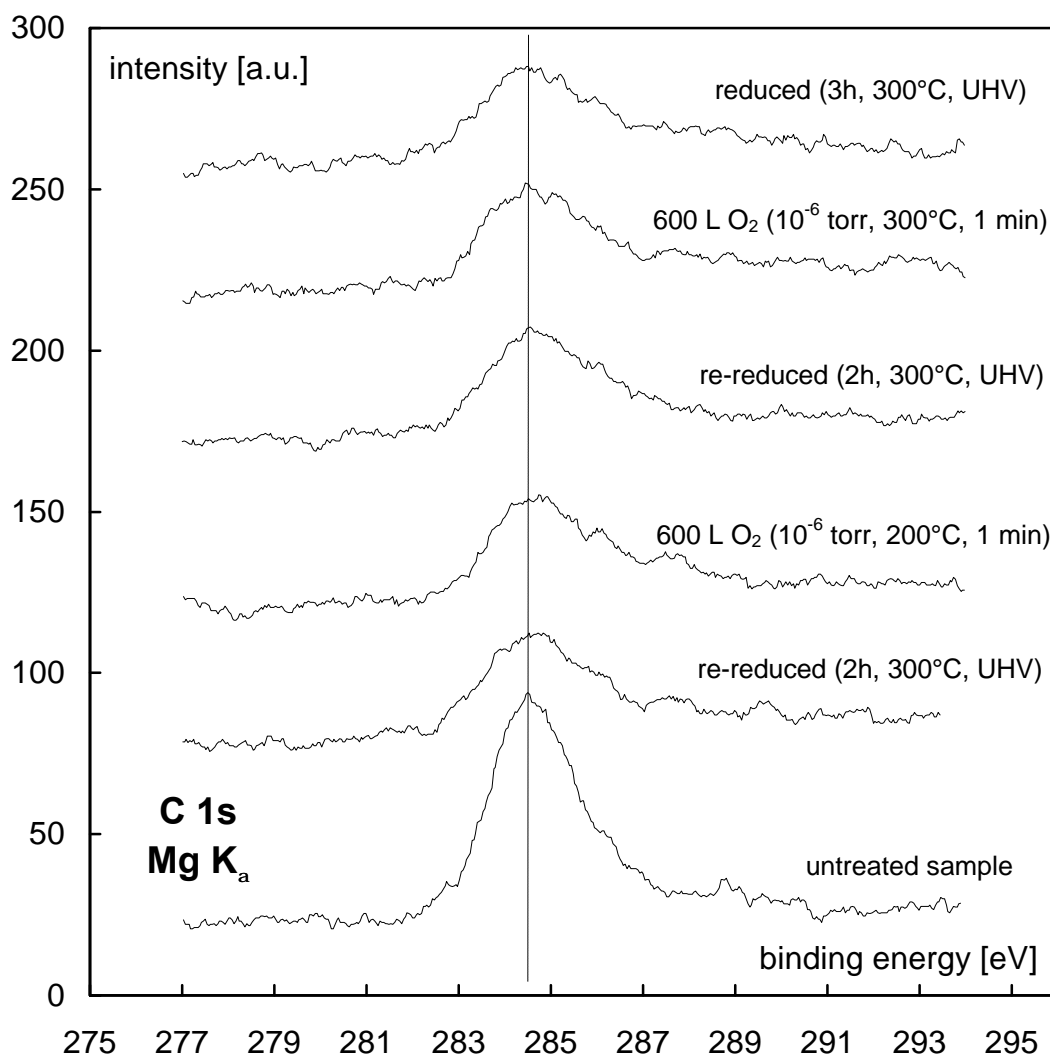

Figure 6.1. Carbon 1s photoemission spectra from the unsupported Cu/Ni alloy particles as a function of the chemical treatments described in the text. The photoemission peak of the carbon contamination in/around the sample was used as the internal XPS energy reference (indicated by the dashed vertical line at 284.4 eV).

spectra was referenced relative to the C 1s photoemission peak of graphitic carbon (284.4 eV), which is present on the sample and/or the supporting Pt foil (fig. 6.1). Resistive heating of the Pt foil allowed temperature variation, and the temperature was followed by a chromel/alumel (T1/T2) thermocouple pressed into the alloy pellet during its preparation.

6.3. Results and Discussion

6.3.1. XPS

After storage in air for a few days, the XPS analysis of the surface composition of the untreated, unsupported particles did reveal the presence of considerable amounts of carbon (fig. 6.1) and oxygen (fig. 6.3), as well as a sodium impurity (fig. 6.2) which had not been removed by washing of the hydroxidic sample precursor. As one would expect, the Ni 2p-region of the XP-spectrum (fig. 6.4) exhibited the characteristics of an oxidised Ni-surface [60]. Fundamental studies of Ni oxidation, both with single crystal surfaces and polycrystalline samples [60] have shown that the uptake of oxygen at room temperature proceeds rapidly to a saturation coverage corresponding to a few monolayers (MLs) of NiO. Further oxidation is kinetically limited by slow Ni-diffusion through the oxide overlayer (tarnishing process) [61,62]. The presence of NiO is also indicated in the O 1s spectrum of the untreated sample (fig. 6.3) which is dominated by features around 532 eV and a strong shoulder at about 530 eV. The latter is characteristic of the oxidic species in NiO. The strong signals on the high binding-energy side of the NiO contribution correspond to impurity states [60], presumably adsorbed hydroxide, carbon monoxide and carbonate. The presence of adsorbed carbon oxide species is in line with the strong C 1s emission from the untreated sample (fig. 6.1). In view of the fact that the sample had been stored and handled in ambient air prior to mounting in the UHV system, it is not surprising that significant amounts of oxidic and carbon contaminants are found. The copious abundance of impurity overlayers also offers a simple explanation for the facts that (i) Ni 2p emission from the sample is quite weak (fig. 6.4) and (ii) Cu can barely be detected (cf. lowest spectrum of fig. 6.5).
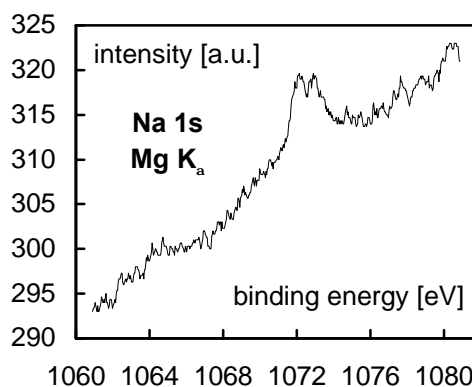

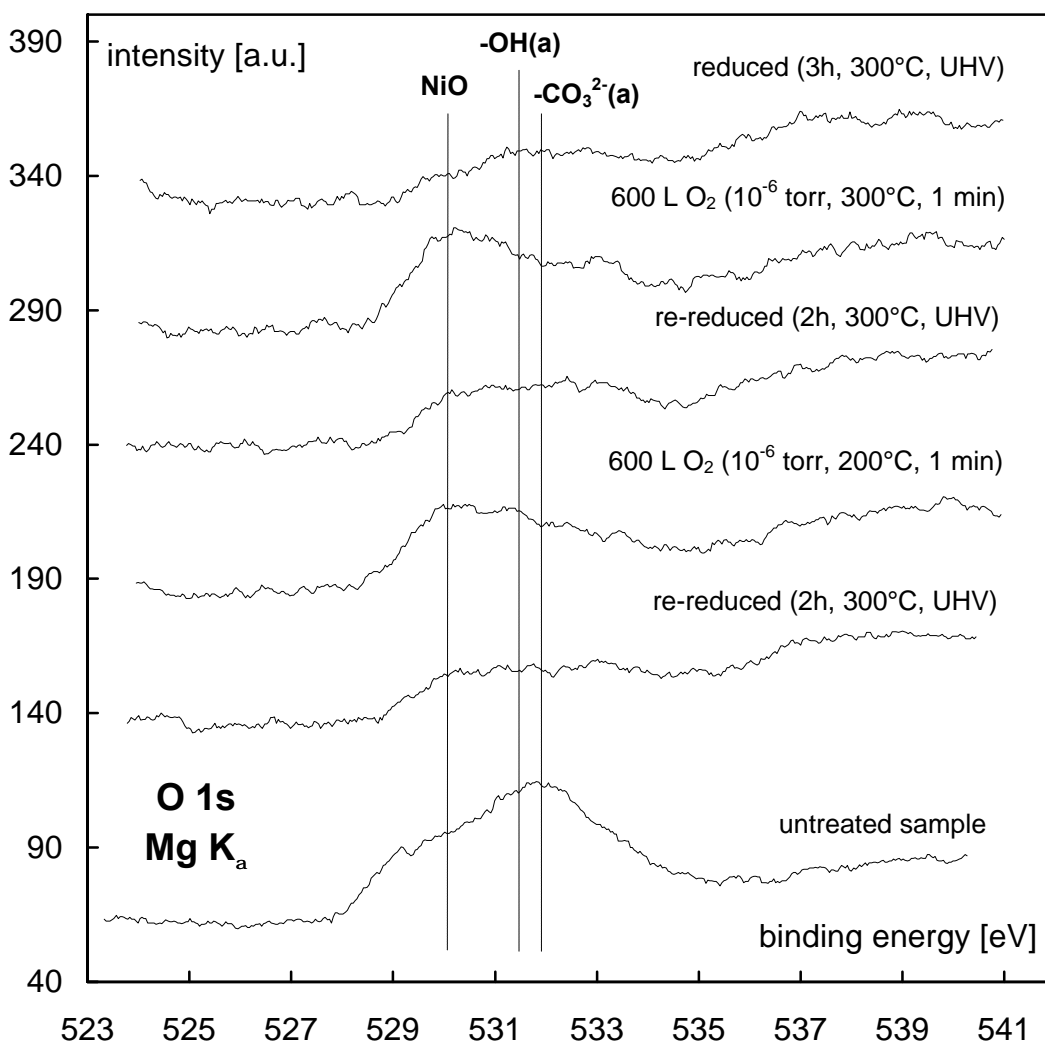**Figure 6.2.**   Na 1s spectrum of the untreated Cu/Ni particles.

Figure 6.3. Oxygen 1s photoemission spectra of the air-exposed, untreated sample (spectrum at the bottom of the figure) and as a function of reduction, re-oxidation, and re-reduction conditions (spectra from top to bottom). The energetic position of photoemission lines due to NiO, adsorbed hydroxide and adsorbed carbonate are indicated by the vertical, dashed lines.

Effective cleaning and reduction of the sample was achieved by prolonged heating (3 h) to 300°C under UHV conditions. The removal of impurities allows the intensity of the Ni 2p emission to increase (fig. 6.4). That reduction of the heat-treated sample is almost complete is borne out by comparison with single crystal Ni XP-spectra reported in the literature [63,64]: most of the inelastic structure at 860 eV - 865 eV has disappeared in favour of compratively sharp Ni 2p peaks followed by the strong shake feature [64] on the high binding-energy side at about 858 eV. Most of the O 1s intensity due to NiO and overlayer species has disappeared (fig. 6.3) - only small residual impurity states can be detected, some of which must be located on the Pt foil (note that strong Pt 4f lines were always detectable by XPS).
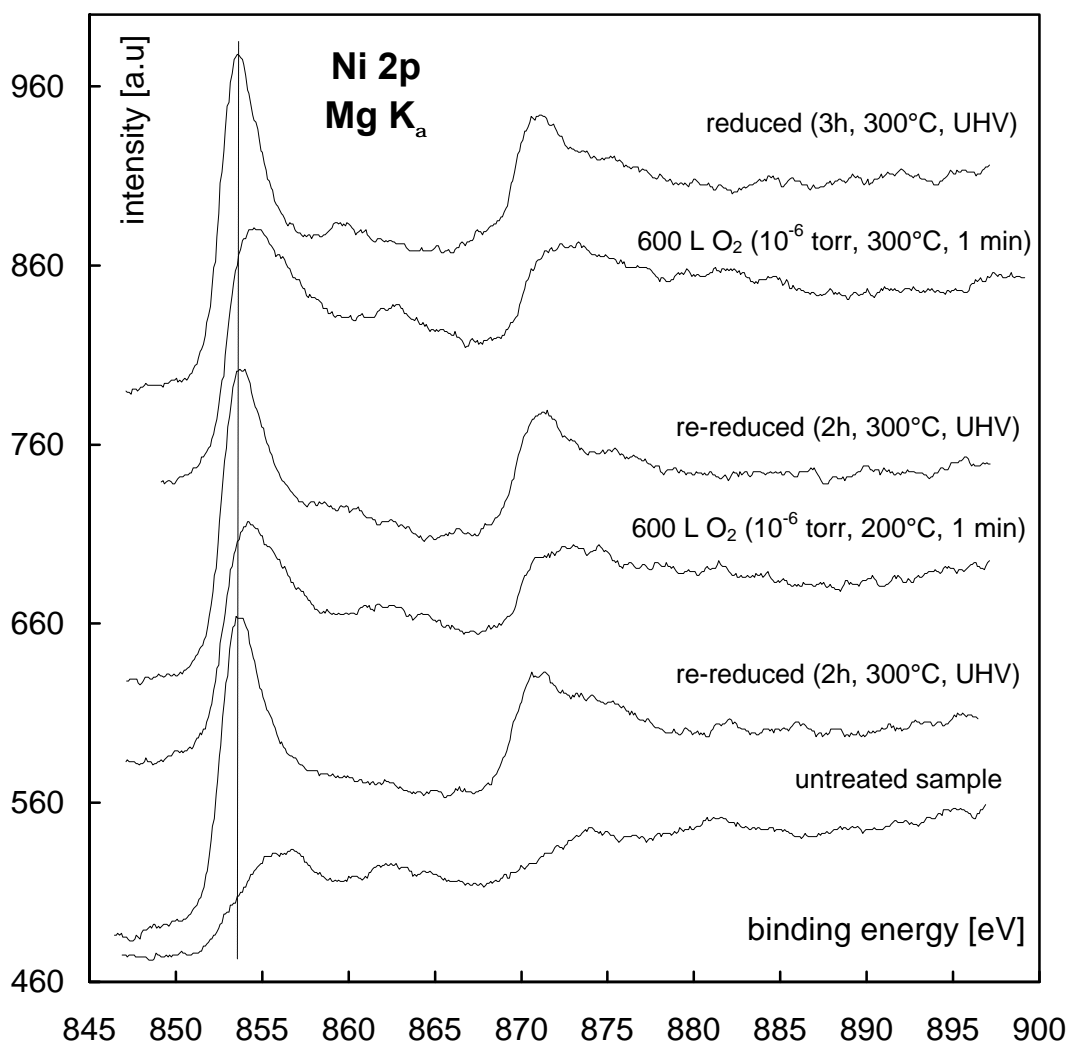
Figure 6.4.   Nickel 2p photoemission spectra of the air-exposed, untreated sample (spectrum at the bottom of the figure) and as a function of reduction, re-oxidation, and re-reduction conditions (spectra from top to bottom). The energetic position of the Ni $2p_{3/2}$ emission line from metallic Ni is indicated by the vertical dashed line.

Examination of the Cu $2p_{3/2}$ region of the XP-spectrum reveals that reduction leads to strong surface segregation of Cu (fig. 6.5). The intensity ratio between the Cu $2p_{3/2}$ and the Ni $2p_{3/2}$ emission peaks was determined from their relative height rather than their areas since the baseline in the Ni 2p spectrum is difficult to establish. The height ratio was found to be 0.75 ± 0.1 (the large error margin allows for the uncertainty in the baseline determination). That this ratio is likely to correspond to a surface enrichment of Cu is indicated by an intensity analysis based on inelastic mean free paths (IMFPs) calculated by the TPP-2 method [65] and empirical, relative atomic emission intensity ("atomic sensitivity") factors tabulated by Wagner *et al.* [66,67]. This effective-medium analysis, which is based on the assumption of exponential depth attenuation and a semi-infinite sample, is quite

standard and is therefore not described here in detail. A discussion of the procedure can be found, e.g., in section 5.4.2. of ref. [68]. The parameters used for the calculations are given in table 6.1.
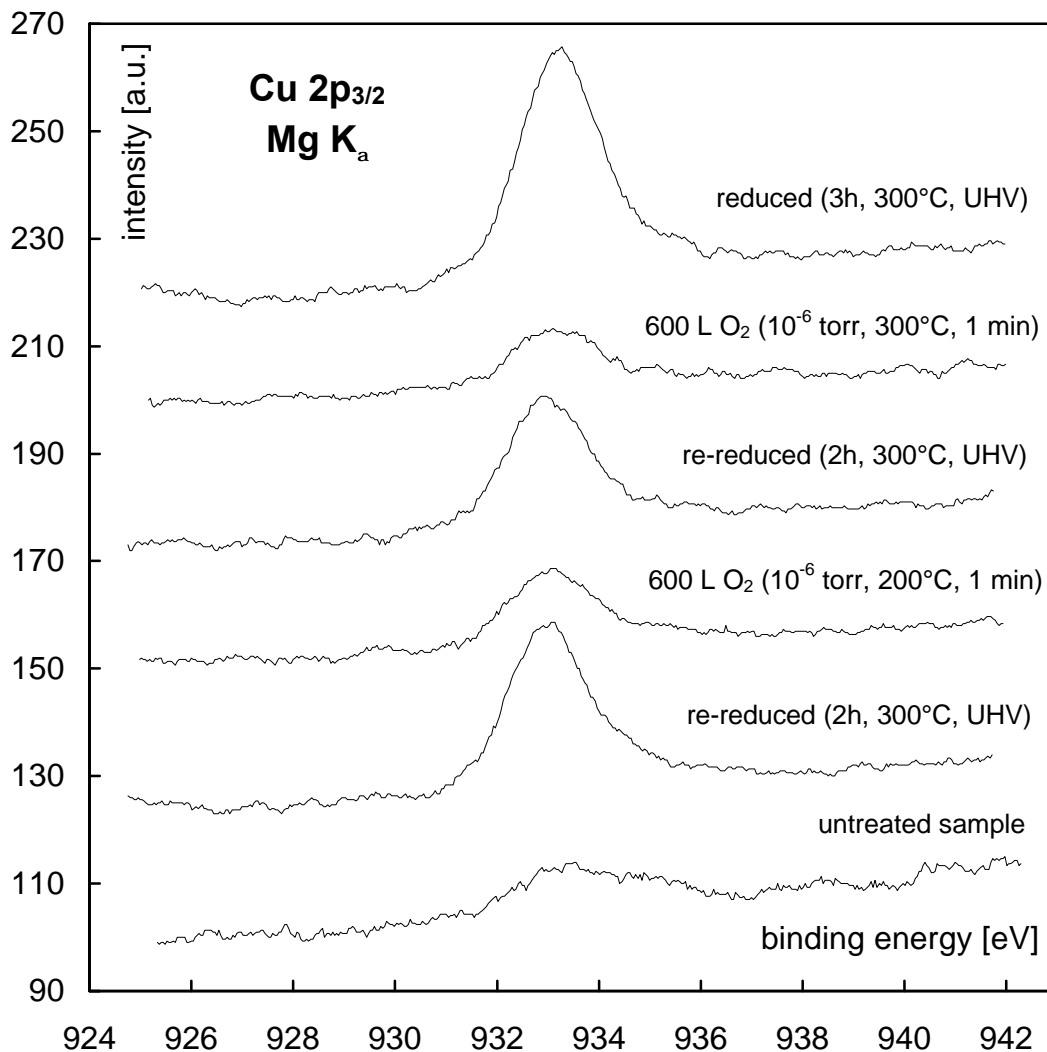

Figure 6.5. Cu $2p_{3/2}$ photoemission spectra of the air-exposed, untreated sample (spectrum at the bottom of the figure) and as a function of reduction, re-oxidation, and re-reduction conditions (spectra from top to bottom).

The predicted dependence of the Cu:Ni emission intensity ratio on the amount of segregated Cu present at the surface of the Cu$_5$Ni$_{95}$ alloy is shown in fig. 6.6. It can be seen that the experimental intensity ratio of 0.75 actually *exceeds* all calculated values by a quite significant margin. Even for a full monolayer, the calculation predicts the Cu 2p$_{3/2}$ peak height to be less than about 40% of the height of the Ni 2p$_{3/2}$ emission line. The apparent discrepancy can probably be resolved by taking account of three important factors neglected by the calculation. Firstly, the enhanced surface-to-volume ratio of small particles amplifies the surface- relative to the bulk-signal. Secondly, the height of the Ni 2p$_{3/2}$ line depends critically on the oxidation state of the Ni atoms. Comparison with spectra given in the literature, e.g., in ref. [63], indicates that Ni^{2+} contributions to the spectrum of the heat-treated Cu$_5$Ni$_{95}$ alloy are still of the order of at least 10%.

Thirdly, the model calculation assumes that the surface segregation effect is sufficiently described by the formation of a monatomic overlayer. However, enrichment of the subsurface region is also likely when segregation occurs and has actually been observed in single crystal studies [22]. Previous work with single crystals of Cu$_5$Ni$_{95}$ alloys indicated Cu surface concentrations of 0.6 - 0.95 monolayers (cf. refs. [20,22,36]). When all these corrections are taken into account then the experimentally determined value matches the calculated ratio for a full segregated monolayer more closely. The calculated Cu:Ni ratio should be regarded as a lower limit to the Cu:Ni intensity ratio under segregation conditions. The relatively high intensity of the Cu 2p$_{3/2}$ emission line is
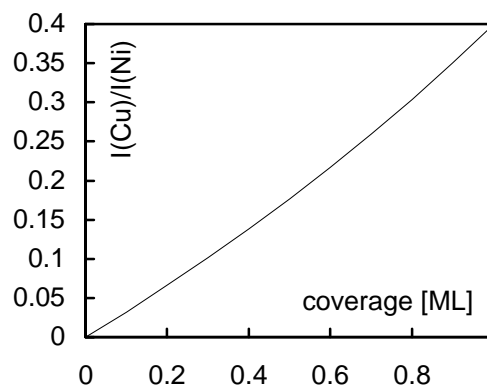

Figure 6.6.   Calculated Cu:Ni 2p$_{3/2}$ emission intensity ratio as a function of monolayer coverage for a semi-infinite sample.

Table 6.1.   Parameters for the intensity calculation presented in figure 6.6.

	Cu 2p$_{3/2}$	Ni 2p$_{3/2}$
electron energy [eV]	930 eV	850 eV
IMFP [65]	10 Å	11 Å
atomic sensitivity factor [66]	4.2	3
detection angle	45°	
X-ray incidence angle	30°	

therefore good evidence for the enrichment of Cu in the surface region of the dispersed alloy.

Further evidence for a strong segregation effect comes from the dynamic changes in the Cu 2p spectrum during surface reacitivity experiments with oxygen. Exposure of the clean and reduced alloy particles to 600 L of oxygen at temperatures between 200°C and 300°C restores the particle surface to an oxidised state (fig. 6.4). Concomitant with surface oxidation, the intensity of the Cu emission decreases substantially (fig. 6.5). Obviously, the oxidation process is accompanied by scrambling of the Cu and Ni atoms. This mixing process during oxidation of Cu/Ni alloys was established by previous work [16,19,44] and is fully reversible *via* re-reduction of the surface (cf. figs. 6.3 to 6.5). Note that re-reduction of the particles oxidised at elevated temperature required much longer periods of time than the initial reduction of particles which had been stored in air at room temperature. This suggests either that a thicker or a more stable oxide layer has been formed than at room temperature. Because of the limited probing depth of XPS, the actual thickness of the oxide layers is difficult to estimate. However, a limiting value has been provided by previous studies of the oxidation of single-crystalline Ni surfaces at 400°C, which show that the reaction with oxygen slows down after an approximately 20 Å thick film of NiO has formed [60].

In summary, the XPS measurements established that Cu segregation occurs in the alloy particles after thermal equilibration at 200°C - 300°C. Furthermore, the concentration of Cu at the surface can be varied as a function of the oxidation state in the near-surface region of the particles.

6.3.2. XRD

The XRD patterns of the untreated (air exposed at room temperature), the reduced and a reoxidised (300°C, air, 30 min) sample exhibit broadened lines for which a full line-shape analysis indicates alloy particle sizes between 160 Å and 240 Å (fig. 6.7). Note that the distribution functions also indicate that oxidation of the smallest particles proceeds much more readily than that of the contributors with larger diameters. Note further that reduction of the previously air-exposed unsupported alloy powder also leads to some sintering, as indicated by the larger average diameter of the particles.

Knowledge of the particle size enables an estimation of the amount of bulk depletion of Cu as a result of segregation. The relation between the surface atom fraction and particle diameters has already been discussed in section 5.3. of the preceding chapter
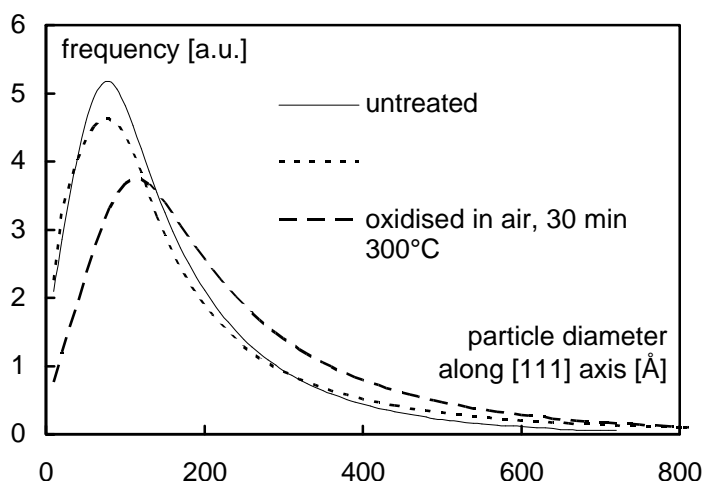
Figure 6.7. Particle size distribution functions determined by a lineshape analysis of the (111) reflection of the nanocrystalline Cu_5Ni_{95} allow powders as a function of chemical treatment. The average particle sizes for the three samples are 157 Å (untreated), 192 Å (reduced) and 239 Å (oxidised).

(cf. fig. 5.14). The line-broadening analysis indicates a substantial fraction of particles to have diameters below 200 Å. For such particles, surface atoms constitute a few percent of the total number of atoms contained within the particles. As a result, the bulk concentration of Cu must decrease substantially when segregation to the surface occurs. In fact, for spherical particles with a diameter below approximately 200 Å the Cu concentration of 5% would almost certainly not suffice to enable the formation of a full Cu overlayer.

6.3.3. XAFS

An interesting point is whether segregation phenomena can be studied by TEY XAFS. TEY XAFS detection of changes in the alloy composition could take advantage of the following effects:

(i) The nearest neighbour distances around the absorbers should vary as a function of the degree of segregation. The lattice constant of the alloy (fcc structure) should be close to that of metallic fcc-Ni (a = 3.52 Å) rather than Cu (a = 3.61 Å) as Cu/Ni alloys follow Vegard's rule quite accurately [6]. If segregation of Cu occurred then the local environment of the Cu absorbers should exhibit lattice widening.

(ii) Surface segregation of Cu may become noticeable as a reduction of its coordination number and/or changes in the Debye-Waller factor.

(iii) The TEY signal intensity of the segregated Cu atoms should be slightly higher than that of the bulk constituents. This possibility has previously

been considered by Sinfelt and co-workers studying Cu/Ni alloys in UHV by soft TEY XAS at the L-edges of Cu and Ni [41,43]. It will be further discussed below.

XAFS spectra of the alloy sample previously characterised by XPS were therefore obtained for both the untreated state and following reduction (300°C, 2 h) in a H$_2$ atmosphere. Strong monochromator glitches limited the available energy range for the Cu K-edge data to 10 Å^{-1}. Furthermore, the strong background absorption due to the Ni-edge amplified beamline and monochromator noise substantially. The noise quality and limited energy range of the Cu data did not allow a multishell analysis as carried out in the previous chapter. The analysis was therefore performed using only the single-scattering nearest-neighbour information contained in the EXAFS. The single shell spectra were obtained by Fourier filtering of the raw data with a Hanning window from 1.5 Å to 2.9 Å. The analysis was performed by first fitting Ni and Cu standard data (obtained by transmission detection) to obtain values for the amplitude factor S_0^2, which were then used for the analysis of the alloy data. The analysis of the Ni K-edge data utilised the same phase shift parameters as for the pure Ni foil. In contrast, the potential- and phase shift calculations for the Cu absorption of the alloy considered Cu as an impurity in a Ni lattice. It was verified, however, that treating the central Cu atom as a Ni atom in a Ni environment did not change the fit results for the Cu spectra significantly (except for Fermi level shifts of ± 3 eV). However, considering the Cu component of the alloy as a pure Cu phase did consistently lead to worse fits. These results can be taken as evidence that phase separation between Cu and Ni does not occur. Two representative spectra and the best single scattering fits obtained by the described methods are presented in fig. 6.8.
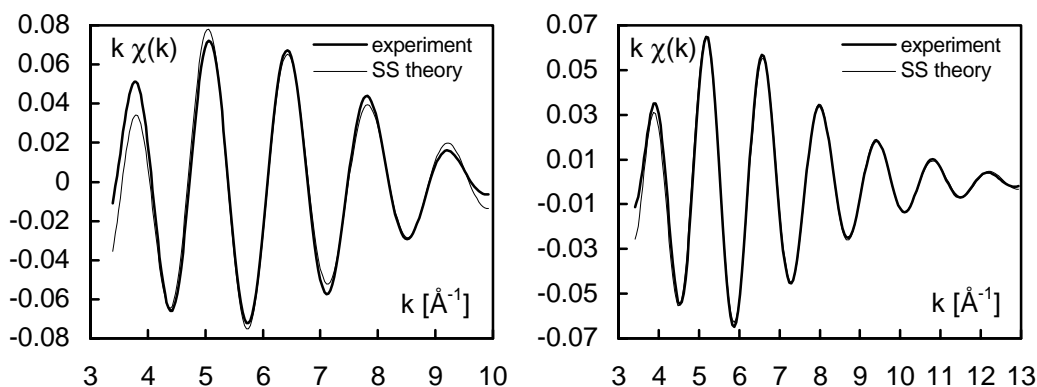

Figure 6.8.   Fourier filtered nearest neighbour data obtained from the EXAFS data for the untreated catalyst. Left Cu data. Right: Ni data.

Table 6.2.   Results of the nearest neighbour single-scattering analysis. All nearest neighbour data were obtained by Fourier filtering of the spectrum with a Hanning window (boundaries: 1.5 - 2.9 Å).

	edge	S_0^2	N_1	R_1 [Å]	s_1^2	k-range	R-factor
Ni foil	Ni	0.82	12	2.482 (1)	0.0118 (3)	3 -13	6
untreated	Ni	0.82	8.8 (1)	2.487 (1)	0.0108 (3)	3 - 13	8
reduced	Ni	0.82	8.7 (1)	2.484 (1)	0.0112 (3)	3 - 13	7
Cu foil	Cu	0.86	12	2.534 (1)	0.0163 (3)	3 - 13	6
untreated	Cu	0.82	11.1 (3)	2.501 (2)	0.0149 (7)	3 - 10	16
reduced	Cu	0.82	8.9 (4)	2.497 (3)	0.0075 (8)	3 - 10	19

Representative results of a fitting analysis of the data are summarised in table 6.2. A well-understood feature of the obtained parameters is the fact that the nearest-neighbour distance around the Cu atoms is more characteristic of a pure Ni- than a Cu-lattice. This result proves that complete desegregation of Cu and Ni into separate phases has not occurred during the experiments. Closer inspection shows also that the nearest-neighbour spacing from the viewpoint of Cu is approximately 0.01 Å longer than the corresponding nearest-neighbour distance around the Ni atoms. While this difference is undoubtedly close to the accuracy limit of XAFS, especially for an analysis based on calculated rather than experimental phaseshifts, it must be stressed that it is obtained irrespective of the choice of the mentioned lattice models (Cu-in-Ni vs. Ni-in-Ni vs. Cu-in-Cu) in the phaseshift calculation. The slight lattice widening around the Cu atoms can therefore be taken as good evidence that the average environment of the Cu atoms is enriched in Cu. This observation would be compatible with the XPS result that the surface concentration of Cu is enhanced and would indicate that the nearest-neighbour environment of the average Cu atom contains approximately 20% Cu atoms.
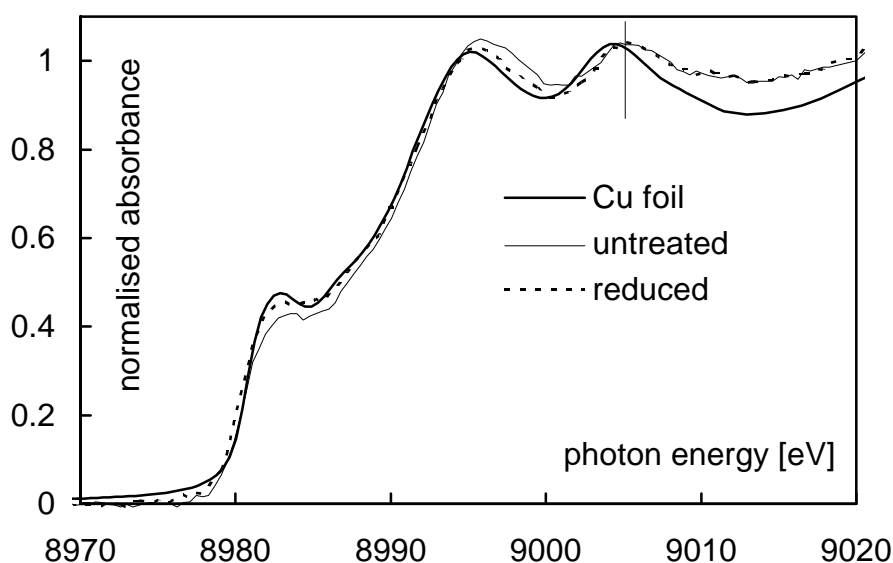
Figure 6.9.   Pre-edge subtracted, normalised Cu K-edge XANES data of a Cu foil (thick line, transmission), the untreated alloy sample (thin line, TEY) and the same alloy sample reduced in H_2 at 300°C for 30 min (dotted line).

The absence of complete desegregation is also indicated by the XANES regions of the spectra. After aligning all Cu spectra at the first edge-step inflection point (an absolute energy calibration is not possible with the TEY detection setup), energy shifts between the positions of the XAFS maxima of the alloy data relative to the spectrum of bulk Cu are clearly visible (fig. 6.9). A similar shift is not discernible in the corresponding Ni XANES data (fig. 6.10). The lower frequency of the near-edge XAFS oscillations in the alloy data indicates a smaller distance to the backscatterers in the alloy environment than in pure Cu metal. Interestingly, the near-edge structure of the reduced alloy appears to correlate better with pure Cu than does the untreated sample. The difference is particularly striking in the energy range between 8978 eV and 8988 eV.

The presence of residual EXAFS oscillations due to Ni is responsible for the fact that a reliable normalisation and post-edge background subtraction of the Cu data have so far proved impossible. The problems encountered are illustrated in fig. 6.11 which shows that a strong Ni EXAFS oscillation dominates the pre-edge region. Furthermore, the Cu K-edge is located in the rising part of an oscillation so that normalisation of the background is somewhat arbitrary. The resulting distortion in the background of the near-edge spectrum is indicated in fig. 6.11. Note particularly the 'offset' of the EXAFS region which is introduced by the oscillatory background component.
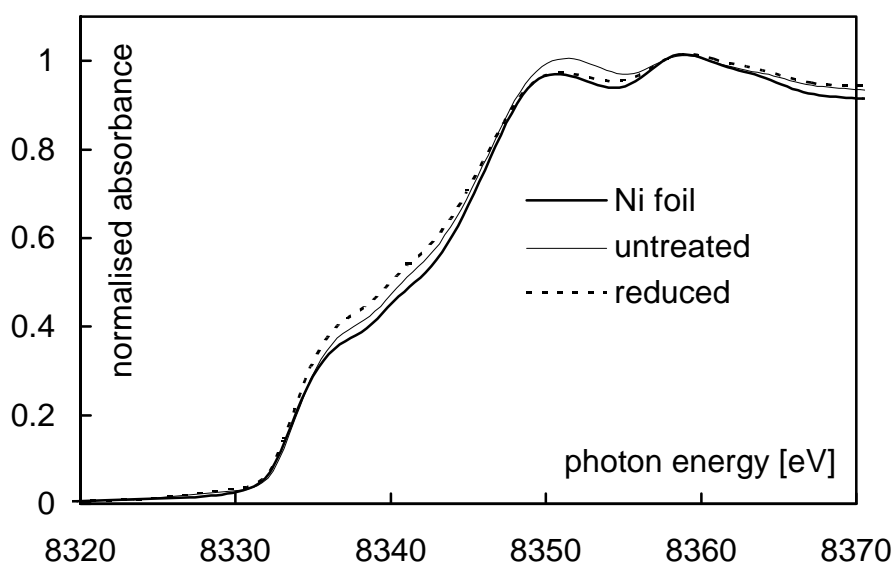
Figure 6.10.   Pre-edge subtracted, normalised Ni K-edge XANES data of a Cu foil (thick line, transmission), the untreated alloy sample (thin line, TEY) and the same alloy sample reduced in H_2 at 300°C for 30 min (dotted line).

Due to the uncertainties introduced by the background subtraction, the amplitude information in the Cu EXAFS of the alloy is not well understood at the time of writing. Turning to the best-fit results presented in table 6.2, one notes that the nearest-neighbour coordination number around the Cu component seems to decrease upon reduction of the sample. Furthermore, the Debye-Waller factor appears to halve as a result of the treatment. This might indicate strain in the segregated Cu lattice which exhibits essentially the lattice constant of Ni. That these results are not very reliable, however, is indicated by the fact that the quality of the fits to the single-shell Cu data of the alloy is very unsatisfactory. Part of the reasons for the bad fit is the very limited k-space range of the data. This was confirmed by a comparative analysis using the Ni K-edge data of the alloy. Limiting the k-space window of the Ni K-edge data to 10 Å⁻¹ and performing a single-shell analysis of the Fourier filtered nearest-neighbour spectrum yielded much worse fits to the data than an analysis based on a maximum k-value of 13 Å⁻¹. The underlying reason is that Fourier filtering does not separate the first shell spectrum from the contributions of the second shell in the fcc lattice reliably. Furthermore, the presence of the Ni EXAFS introduced a low-frequency component into the data which overlapped with the nearest-shell component of the Cu data. Filtering problems therefore explain at least part of the unsatisfactory fits to the Cu data. A better dataset for the Cu component is necessary to perform a reliable analysis of the amplitude information. Note that the nearest-neighbour information in the data is unaffected by the normalisation problems.
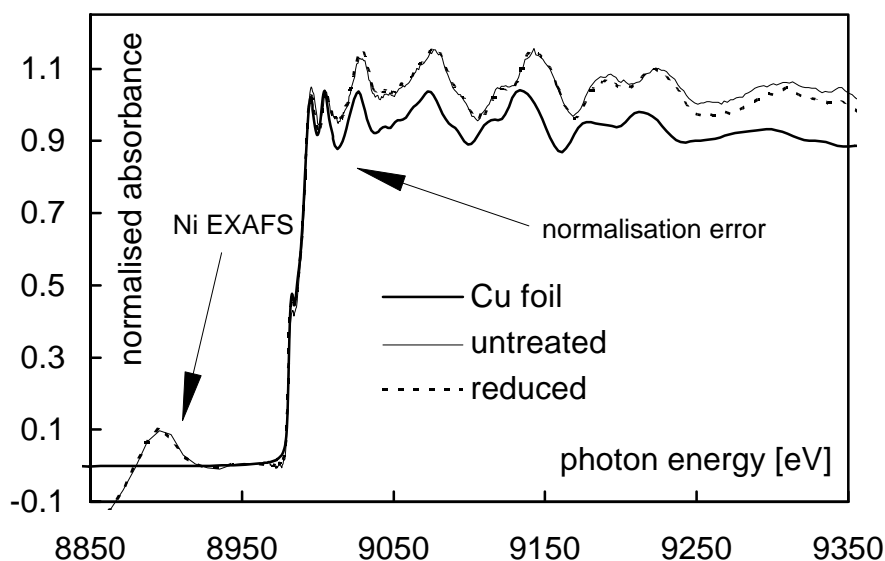
Figure 6.11.   Pre-edge subtracted, normalised Cu K-edge data of a Cu foil (thick line, transmission), the untreated alloy sample (thin line, TEY) and the same alloy sample reduced in H_2 at 300°C for 30 min (dotted line).

Finally, inspection of table 6.2 reveals that the coordination numbers of the Ni component are significantly reduced as compared to the Ni metal standard. Part of the amplitude reduction is probably due to Ni atoms at the surface of the smallest particles in the sample. A reduction by approximately 5% is also expected arising from the fluorescence-related 'self'absorption' effect (cf. chapter 4). However, the observed reduction of the amplitude is approximately 25% - too large to be compatible with the surface atom fraction factor and the fluorescence-yield effect. This raises the possibility that the remaining part of the amplitude reduction is therefore due to a 'self-absorption' effect related to particle size effects and/or surface roughness. Future work certainly has to address the question whether such an effect exists, if it is responsible for the low Ni K-edge amplitudes, and how it can be predicted quantitatively.

6.3.4. Edge Step Heights

The edge jump height in the K-shell spectra is a measure of the number of atoms probed by the X-ray absorption measurement. Analysis of the Cu and Ni K-edge step ratios in the alloy data consistently indicated an enhanced contribution of Cu atoms as compared to the EDX-derived molar fraction ratio of 0.06 in the particles (fig. 6.12). Since XPS has shown that the surface of the reduced Cu/Ni alloy particles is enriched in Cu, the enhancement of the Cu/Ni signal ratio might be taken as evidence that the surface sensitivity of electron yield detection is high enough to probe the segregated layer preferentially.
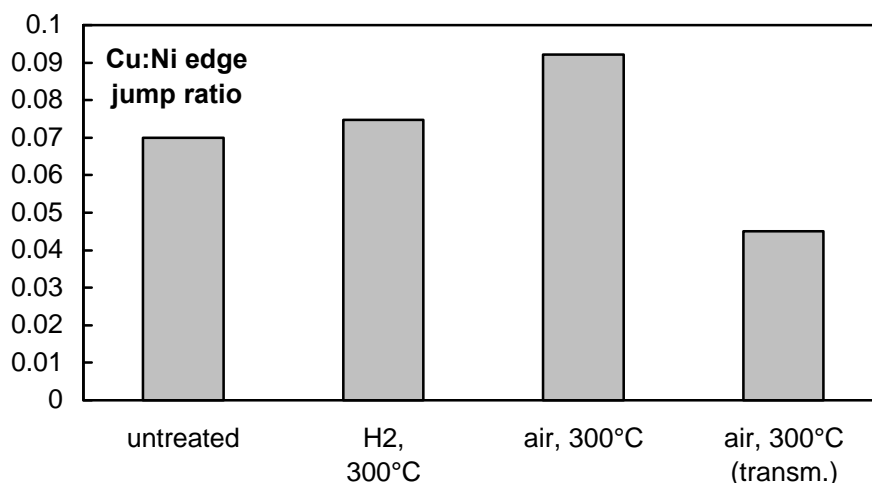
Figure 6.12.   Cu/Ni edge jump ratios for the alloy particles in dependence on ambient gas treatment.

Care must be taken, however, not to overinterpret these data because several additional factors favour the Cu signal over the Ni contribution. The most important among these is the increasing transmission of the ionisation chamber used for the measurements. The chamber had a length of 20 cm and was filled with an Ar atmosphere of 40 mbar. Figure 6.13. shows that the mass absorption coefficient of Ar decreases by approximately 20% between the Ni- (8.33 keV) and the Cu-edge (8.99 keV). The right diagram of fig. 6.13 shows that this decrease translates into an increase of the X-ray intensity at the sample by a factor of 1.03. The ionisation chamber current used for the normalisation of the spectrum decreases by the inverse value (to 0.97). Similarly, the transmission of the air path between the ionisation chamber and the sample (approximately 20 cm) increases by a factor of 1.04 (fig. 6.13). The transmission change of the Be windows at the exit of the ionisation chamber and the entrance to the TEY cell is negligible. Not negligible, however, is the difference in the KLL Auger electron energies emitted from Ni (6.5 keV) and Cu (7 keV). Their ratio adds an amplification factor of 1.08 in favour of the Cu edge. Multiplying the four correction factors results in a total amplification factor of

$$1.04 \times 1.08 \times 1.03 \,/\, 0.97 \approx 1.19,$$

indicating that the observed edge step ratios of 0.72 ± 0.02 do not derive from segregation effects.
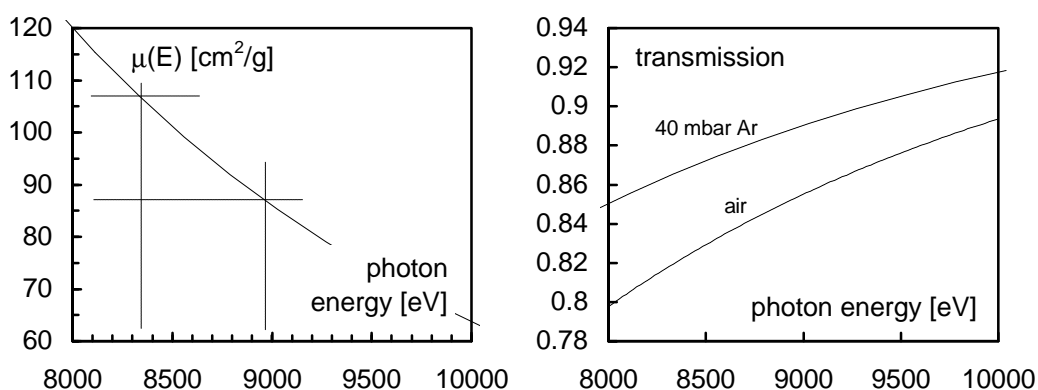
Figure 6.13. Change of the X-ray mass absorption coefficient of Ar (left diagram) and the transmission of 40 mbar of Ar and 1 atm of air along a pathlength of 20 cm.

A check was made to demonstrate that the enhanced edge-jump ratio was indeed intrinsic to the TEY measurement. A sample of the alloy was oxidised in a stream of blended air for 30 min at 300°C. This procedure passivates the sample enough to handle it *ex situ* without any possibility of morphology changes due to air exposure. After taking an *in situ* TEY spectrum the sample was therefore removed from the TEY cell, ground in a mortar, and diluted with boron nitride. An additional EXAFS measurements was carried out in transmission mode using a sample with an effective absorbance of $\Delta\mu\ x = 0.9$. As transmission detection probes the whole particle volume, the edge jump ratio is more representative of the particle composition to within an error margin of approximately 20%.

Interestingly, an enhancement of the Cu:Ni edge jump ratio was observed in the TEY spectrum of the oxidised sample. This result might seem unexpected, as XPS had indicated extensive intermixing between Cu and Ni after oxidation in UHV. It should be kept in mind, however, that the probing depth characteristics of XPS and TEY XAFS are very different. The oxidative treatment of the alloy in UHV could lead to sufficient intermixing between Cu and Ni on the probing depth scale of XPS (< 10 Å). By contrast, the TEY XAFS measurement would only exhibit an enhanced edge jump if near-surface enrichment of one alloy component occurred on a scale of approximately 100 Å. The observed TEY edge step ratio of about 0.9 thus suggests that the scale formed in air during oxidation at 300°C is enriched in Cu. That the scale thickness must be quite substantial is indicated by the fact that the oxide overlayer attenuates the K-edge emission from the metallic core of the particles quite efficiently (fig. 6.14). This is reinforced by the higher intensity of the 'white line' of the TEY spectrum from the Cu K-edge and also by the damping of the residual Ni EXAFS in the pre-edge region. Remember also that the XRD line-broadening analysis indicated additional sintering of the metal particles during oxidation (fig.
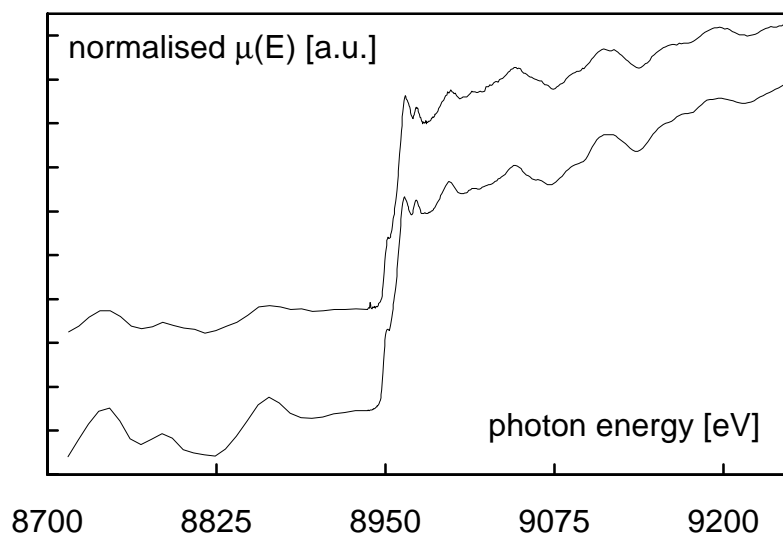
Fig. 6.14. Preedge background subtracted and normalised transmission (lower spectrum) vs. TEY (upper spectrum) data for the Cu K-edge of the alloy particles. The reduction of the residual amplitude from the Ni K-edge in the preedge region of the TEY data is due to the attenuation of the strong alloy XAFS by the oxide overlayer. Note also that the 'white line' intensity in the near-edge of the TEY spectrum is enhanced relative to the transmission data.

6.11). As a result, 'self-attenuation' of the metal contribution to the XAFS should become more important.

6.4. Summary

The presented explorative study of Cu_5Ni_{95} alloy particles has shown how TEY XAFS can be exploited to study surface enrichment phenomena and reactions *in situ*. Apart from the background subtraction problems encountered during analysis of the Cu-edge, the study has also demonstrated some difficulties which are associated with TEY detection. The foremost problem in studies of the metallic particles is still the uncertainty related to the possible presence of 'self-absorption' effects previously unaccounted for. Problems might arise with particles sizes that are 'transparent' for the Auger electrons responsible for the TEY signal. XANES calculations similar to those presented in chapter 5 could be helpful in determining whether the near-edge changes visible in the Ni K-edge data are intrinsic to the sample or an artefact of the measurement.

To resolve some of the uncertainties encountered in this study, additional work in the future could address several outstanding questions. XRD could be employed to verify the slight anisotropy in the lattice parameter of the particle region which are enriched and deficient in Cu. These measurements require a highly accurate calibration of the diffractometer which is currently not possible with the available *in situ* cell. The

background subtraction problem in the Cu XAFS data could be adressed by subtracting a spectrum of pure Ni from the data - a procedure which would require highly accurate XAFS data of an appropriate Ni sample.

6.5. References

[1] C. Mukoid, S. Hawker, J.P.S. Badyal, R.M. Lambert, Catal. Lett. 4 (1990) 57.

[2] P.H. Emmett, N. Skau, J. Am. Chem. Soc. 65 (1943) 1029.

[3] W.K. Hall, P.H. Emmett, J. Phys. Chem. 62 (1958) 816.

[4] R.S. Mann, A.M. Shah, Can. J. Chem. 48 (1970) 3324.

[5] R.S. Mann, K.C. Khulbe, Can. J. Chem. 48 (1970) 2075.

[6] K.C. Khulbe, R.S. Mann, Catal. Rev. - Sci. Eng. 24 (1982) 311.

[7] *Catalyst Handbook* (Wolfe Publishing Ltd. London, 1989).

[8] J.H. Sinfelt, J.L. Carter, D.J.C. Yates, J. Catal. 24 (1972) 283.

[9] D.A. Fischer, G.G. Cohen, N.J. Shevchik, J. Phys. F 10 (1980) L139.

[10] G. Tréglia, B. Legrand, P. Maugain, Surf. Sci. 225 (1990) 319.

[11] O.L.J. Gijzeman, J. Catal. 92 (1985) 409.

[12] C.T. Campbell, Ann. Rev. Phys. Chem. 41 (1990) 775.

[13] P. Wynblatt, R.C. Ku, Surf. Sci. 65 (1977) 511.

[14] M.-L. Shek, Surf. Sci. Lett. 149 (1985) L39.

[15] T. Berghaus, C. Lunau, H. Neddermeyer, V. Rogge, Surf. Sci. 182 (1987) 13.

[16] L.E. Rehn, H.A. Hoff, N.Q. Lam, Phys. Rev. Lett. 57 (1986) 780.

[17] N.Q. Lam, H.A. Hoff, H. Wiedersich, L.E. Rehn, Surf. Sci. 149 (1985) 517.

[18] J. Egelhoff, Phys. Rev. Lett. 50 (1983) 587.

[19] K. Wandelt, C.R. Brundle, Phys. Rev. Lett. 46 (1981) 1529.

[20] Y.S. Ng, T.T. Tsong, J. McLane, Phys. Rev. Lett. 42 (1979) 588.

[21] Y.S. Ng, T.T. Tsong, J. McLane, Surf. Sci. 84 (1979) 31.

[22] P.R. Webber, C.E. Rojas, P.J. Dobson, D. Chadwick, Surf. Sci. 105 (1981) 20.

[23] D.T. Ling, J.N. Miller, I. Lindau, W.E. Spicer, P.M. Stefan, Surf. Sci. 74 (1978) 612.

[24] H.H. Brongersma, M.J. Sparnaay, T.M. Buck, Surf. Sci. 71 (1978) 657.

[25] F. Chehab, W. Kirstein, F. Thieme, Surf. Sci. 152/153 (1985) 367.

[26] W.D. Roos, G.N. van Wyk, J. du Plessis, Surf. Interface Anal. 20 (1993) 95.

[27] E.M. Silverman, R.J. Madix, D.T. Ling, W.E. Spicer, Chem. Phys. Lett. 71 (1980) 452.

[28] E.M. Silverman, R.J. Madix, P. Delrue, Surf. Sci. 109 (1981) 127.

[29] D.H.S. Ying, R.J. Madix, Prepr. - Can. Symp. Catal. 5th (1977) 317.

[30] D.H.S. Ying, R.J. Madix, J. Catal. 60 (1979) 441.

[31] E.M. Silverman, R.J. Madix, J. Catal. 56 (1979) 349.

[32] D.H.S. Ying, R.J. Madix, Inorg. Chem. 17 (1978) 1103.

[33] L.E. Rehn, S. Danyluk, H. Wiedersich, Phys. Rev. Lett. 43 (1979) 1764.

[34] N.K. Allen, P.J. Durham, B.L. Gyorffy, R.G. Jordan, J. Phys. F 13 (1983) 223.

[35] H.H. Brongersma, P.A.J. Ackermans, A.D. van Langeveld, Phys. Rev. B 34 (1986) 5974.

[36] P.R. Webber, M.A. Morris, Z.G. Zhang, J. Phys. F 16 (1986) 413.

[37] P.R. Webber, Z.G. Zhang, M.A. Morris, J. Phys. F 15 (1985) 249.

[38] T. Sakurai, Phys. Rev. Lett. 57 (1986) 781.

[39] T. Sakurai, T. Hashizume, A. Kobayashi, A. Sakai, S. Hyodo, Y. Kuk, H.W. Pickering, Phys. Rev. B 34 (1986) 8379.

[40] T. Sakurai, T. Hashizume, A. Jimbo, A. Sakai, S. Hyodo, Phys. Rev. Lett. 55 (1985) 514.

[41] J.H. Sinfelt, G.D. Meitzner, Acc. Chem. Res. 26 (1993) 1.

[42] C.A. Bernardo, I. Alstrup, J.R. Rostrup-Nielsen, J. Catal. 96 (1985) 517.

[43] G. Meitzner, D.A. Fischer, J.H. Sinfelt, Catal. Lett. 15 (1992) 219.

[44] G.U. Kulkarni, G. Sankar, C.N.R. Rao, J. Catal. 131 (1991) 491.

[45] J.R. Rostrup-Nielsen, *Catalytic Steam Reforming,* in: Catalysis, Science and Technology Vol.5, ed. by J.R. Anderson and M. Boudart (Springer Verlag, Berlin, Heidelberg, New York, 1984) 1.

[46] R.M. Friedman, J.J. Freeman, F.W. Lytle, J. Catal. 55 (1978) 10.

[47] J.R. Rostrup-Nielsen, J. Catal. 85 (1984) 31.

[48] N.G. Pilling, R.G. Bedworth, J. Inst. Met. 29 (1923) 529.

[49] K. Hirokawa, T. Sato, M. Oku, Fresenius Z. Anal. Chem. 297 (1979) 393.

[50] J.A. Dalmon, G.A. Martin, *CH4, C2H6 and C3H8 Formation in CO + H2 Reaction over Supported on Silica Nickel and Nickel-Copper Catalysts,* in: New Horizons in Catalysis, Proceedings of the 7th International Congress on Catalysis (Studies in Surface Science and Catalysis Vol.7), ed. by T. Seiyama and K. Tanabe (Elsevier, Amsterdam, Oxford, New York, 1981) 402.

[51] J.A. Dalmon, J. Catal. 60 (1979) 325.

[52] Z. Maskos, J.H.C. van Hooff, J. Catal. 66 (1980) 73.

[53] T.S. Cale, J.T. Richardson, J. Catal. 79 (1983) 378.

[54] V. Ponec, Int. J. Quantum Chem. 12, Suppl.2 (1977) 1.

[55] L.J.M. Luyten, M. van Eyck, J. van Grondelle, J.H.C. van Hooff, J. Phys. Chem. 82 (1978) 2000.

[56] G.A. Martin, J.A. Dalmon, J. Catal. 75 (1982) 233.

[57] J.A. Dalmon, G.A. Martin, J. Catal. 66 (1980) 214.

[58] J.A. Dalmon, G.A. Martin, J. Mol. Catal. 25 (1984) 161.

[59] E. Iglesia, M. Boudart, J. Catal. 81 (1983) 204.

[60] C.R. Brundle, J.Q. Broughton, *The initial interaction of oxygen with well-defined transition metal surfaces,* in: The Chemical Physics of Solid Surfaces and Heterogeneous Catalysis Vol.3: Chemisorption Systems, Part A, ed. by D.A. King and D.P. Woodruff (Elsevier, Amsterdam, Oxford, New York, Tokyo, 1990) 131.

[61] C. Wagner, Progress in Solid State Chemistry 10 (1975) 3.

[62] W.W. Smeltzer, D.J. Young, Progress in Solid State Chemistry 10 (1975) 17.

[63] J.P. Espinós, A. Fernández, A.R. González-Elipe, Surf. Sci. 295 (1993) 402.

[64] S.B. Whitfield, G.B. Armen, R. Carr, J.C. Levin, B. Crasemann, Phys. Rev. A 37 (1988) 419.

[65] S. Tanuma, C.J. Powell, D.R. Penn, Surf. Interface Anal. 20 (1993) 77.

[66] C.D. Wagner, L.E. Davis, M.V. Zeller, J.A. Taylor, R.L.H. Gale, Surf. Interface Anal. 3 (1981) 211.

[67] R.J. Ward, B.J. Wood, Surf. Interface Anal. 18 (1992) 679.

[68] M.P. Seah, *Quantification of AES and XPS*, in: *Practical Surface Analysis*, edited by D. Briggs & M.P. Seah (Wiley & Sons, New York 1990), p. 201.